Using novel rigid-fluoride polymer to control the interfacial thickness of graphene and tailor the dielectric behavior of poly(vinylidene fluoride-trifluoroethylene-chlorotrifluoroethylene) nanocomposites

Xianghui Han[a], Sheng Chen*[a], Xuguang Lv[a], Hang Luo[b], Dou Zhang[b], Chris R. Bowen[c]

[a].Key Laboratory of Polymeric Materials and Application Technology of Hunan Province, College of Chemistry, Xiangtan University, Xiangtan 411105, Hunan Province, China

[b].State Key Laboratory of Powder Metallurgy, Central South University, Changsha, Hunan 410083, China

c Department of Mechanical Engineering, University of Bath, Bath, BA2 7AY, UK

Corresponding Authors:

Email: huaxuechensheng@163.com (Sheng Chen)

Abstract: Polymer nanocomposites based on conductive fillers for high performance dielectrics have attracted increasing attention in recent years. However, challenges remain such as filler aggregation and their weak compatibility with the matrix, which significantly limits the potential to enhance permittivity. In addition, a number of physical issues are also unclear, such as the effect of interfacial thickness on the dielectric properties of the polymer nanocomposites. In this research, two core-shell structured reduced graphene oxide (rGO)@rigid-fluoro-polymer conducting fillers with different shell thicknesses were prepared by a surface-initiated reversible-addition-fragmentation chain transfer (SI-RAFT) polymerization method, these were denoted as rGO@PTFMS-1 with a thin shell and rGO@PTFMS-2 with a thick shell. Rigid liquid crystalline fluoride-polymer Poly{5-bis[(4-trifluoro-methoxyphenyl)oxycarbonyl]styrene} (PTFMS) was chosen to tailor the shell thicknesses of rGO for the first time by tailoring the degree of polymerization. The miscibility between the surface functional rGO and polymer matrixes were considerably improved due to the presence of the rigid-fluoride polymers. Dielectric properties of the P(VDF-TrFE-CTFE) nanocomposites with modified rGO were studied in detail and demonstrated that the percolation threshold of the nanocomposites increased from 0.68 vol % to 1.69 vol % with an increase in shell thickness. Compared to the rGO@PTFMS-1/P(VDF-TrFE-CTFE) composites, the rGO@PTFMS-2/P(VDF-TrFE-CTFE) composites exhibited a lower dielectric constant, which can be interpreted by the interfacial polarization and the micro-capacitor model, resulting from the insulating nature of the rigid-polymer shell and the change of rGO morphology. The findings provide an innovative approach to tailor dielectric composites, and promote a deeper understanding of the influence of interfacial regions thickness on the dielectric performance.

1. Introduction

Dielectric materials with high dielectric constant and low dielectric loss play an important part in high performance electronic devices such as radar, electric vehicles, mobile electronics, power electronics, lasers, and rail guns[1-8]. In order to obtain high performance dielectric materials, many strategies have been reported to increase the dielectric constant of the polymers. One approach based on a organic−inorganic hybrid strategy has been extensively studied, in which high dielectric constant (k) nanoparticles are introduced into a polymer matrix. Traditionally, a high filler loading content (often over 50 vol.%) of high-k ceramic fillers such as TiO_2, $BaTiO_3$, $Pb(Zr,Ti)O_3$ and $CaCu_3Ti_4O_{12}$ are added to polymer matrixes[9-12]. However, the issues of inhomogeneity and aggregation of the filler in the polymer matrix due to the high surface energy of dielectric nanoparticles, leads to defects and therefore poor mechanical properties, low flexibility and high density. Conversely, conductive fillers such as Ag, Ni, Zn, $CaCu_3Ti_4O_{12}$, carbon nanotubes (CNTs) and graphene nanosheets (GNs) have been incorporated into the polymer matrix to construct percolated nanocomposites based on percolation theory[13-16]. Near the percolation threshold, the permittivities of nanocomposites are dramatically increased and the nanocomposites simultaneously maintain their processability and mechanical flexibility.

Owing to their excellent electrical, thermal and mechanical properties, GNs and reduced-graphene oxide (rGO) nanosheets have been widely used as a filler to improve the dielectric performance of a polymer[17-19]. However, these fillers readily stack together as a result of the strong Van der Waals'force and the π–π stacking in indiviudal layers and weak interactions with the polymer matrix. These properties, result in a high dielectric loss near the percolation threshold as a result of direct contact between the conductive fillers, and also produce a low breakdown strength

and the energy storage density originating from the defects or voids in the nanocomposite. Thus, it is a significant challenge to achieve a homogenous and stable dispersion of GNs or rGO in a polymer matrix. At present, most of the work to date focuses on chemical functionalization of graphene[20-26]. For example, Chen et al. have reported on a N-(2-hydroxyphenyl)methacrylamide grafted to the rGO via atom transfer radical polymerization (ATRP)[27]. Yang et al. have prepared fluoro-polymer functionalized rGO via self-polymerization of dopamine and subsequent Michael addition of thiol-terminated poly(trifluoroethyl acrylate)[28]. Wu et al. have presented a simple and effective route to form hyperbranched aromatic polyamide functionalized graphene sheets (GS–HBA). The resulting GS-HBA exhibited uniform dispersion in a thermoplastic polyurethane matrix and strong adhesion with the matrix by hydrogen-bond coupling, which improved the load transfer efficiency from the matrix to the rGO[29]. Nandi et al. fabricated poly (methyl methacrylate) (PMMA) functionalized graphene through an ATRP method[30]. Fillers with PMMA on the surface of rGO have excellent compatibility with PVDF and the functionalized rGO can be homogeneously dispersed in a PVDF matrix. Yang et al. have synthesized GROH with a different OH content as well as GRCOOH by means of a diazotizing method, and discussed the dielectric properties of GROH/ PVDF and GRCOOH/PVDF composites[31].

It is worth noting that the current state-of-the-art of interfacial modification is predominantly based on flexible organic small molecules or flexible polymers which collapse on the surface of the modified nanofillers due to random coils so that the thickness and morphology of the interfacial layer cannot be finely tuned[22]. It is well-known that Tanaka et al had proposed a theoretical model for the formation of interfaces either by physical, chemical, or electrical means, when the spherical

nanoparticles are added in the polymer matrix, indicating the thickness of interfacial region has play important role on the dielectric properties of nanocomposites. However, there are few reports that examine in detail the influence of the thickness of the interfacial region on the dielectric properties of nanocomposites based on conducting fillers. Mesogen-jacketed liquid-crystalline polymers (MJLCPs) were firstly synthesized by Zhou et al[32] and the main-chain of the polymer was forced to adopt a stretched conformation due to a strong steric interaction between the polymer main-chain and bulky side chains. Thus, MJLCPs offer a promising opportunity to regulate the rod diameter, surface chemistry and rod length by freely changing the chemistry structure and molecular weight of polymers, which is meaningful to design the chemical structure of interfacial regions and tailor the thickness of interfacial region.

In this paper, we have designed and synthesized the novel mesogen-jacketed liquid crystal polymer (MILCP) Poly{5-bis[(4-trifluoro-methoxyphenyl)oxycarbonyl]styrene} (PTFMS) to tune the interfacial region between rGO and poly(vinylidene fluoride-trifluoroethylene-chlorotrifluoroethylene) P(VDF-TrFE-CTFE). The rigid-fluoro-polymers based on PTFMS possesses a better affinity with the ferroelectric polymer matrix (P(VDF-TrFE-CTFE) and this prevents the rGO nanosheets from agglomerating in the polymer matrix and thereby separates the rGOs to avoid filler contact. In addition, the shell thickness can be controlled by tailoring degree of polymerization via RAFT polymerization and can be calculated via the rod-length of polymer using the following equation (1):

$$L_{rod} = 0.154(nm) \times 2N_{rod} \times \sin 52^\circ \approx 0.24N_{rod}(nm) \quad (1)$$

where N_{rod} is the polymer degree, and L_{rod} is equal to the shell thickness. Using RAFT polymerization, core-shell structured rGO@rigid-fluoride-polymer nanofillers with

two different shell thicknesses were prepared, which were denoted as rGO@PTFMS-1 with a thin shell and rGO@PTFMS-2 with a thick shell. These modified rGOs were introduced into a P(VDF-TrFE-CTFE) polymer matrix. The dielectric properties of the polymer nanocomposites were investigated in detail. The results demonstrated that (i) the dielectric constants of the nanocomposites increase with an increase of the rGO volume fraction under the percolation threshold. (ii) the percolation threshold of the nanocomposites increased from 0.68 vol % to 1.69 vol % with an increase of shell thickness. (iii) compared to the rGO@PTFMS-1/P(VDF-TrFE-CTFE) composites, the rGO@PTFMS-2/P(VDF-TrFE-CTFE) composites exhibited a lower dielectric constant. To the best of our knowledge, this is the first time report on the influence of interfacial region thickness on dielectric behavior of graphene/P(VDF-TrFE-CTFE) nanocomposites.

2. Experiment section

2.1. Materials.

The precursor 2-vinylterephthalic acid (VTA) and RAFT agent 4-cyanopentanoic acid dithiobenzoate (CPDB) were synthesized according to the previous literature[33,34]. P(VDF-TrFE-CTFE) was provided by PolyK Technologies, LLC, USA. N, N-dimethylformamide (DMF), dichloromethane (DCM), and other organic reagents or solvents was supplied by Shanghai Reagents Co. Ltd. N-hydroxysuccinimide (NHS), N,N'-dicyclohexylcarbodiimide (DCC), 4-dimethylaminopyridine (DMAP), and γ-aminopropyl triethoxysilane (γ-APS), 4,4'-azobis(4-cyanovaleric acid), 4-(trifluoromethoxy)phenol were purchased from Acros. Graphene were supplied by.

2.2. Synthesis of monomer 2,5-bis[(4-trifluoromethoxyphenyl)oxycarbonyl]styrene

The synthetic route of the monomer 2,5-bis[(4-trifluoromethoxyphenyl)oxycarbonyl]styrene (TFMS) is shown in **Scheme 1**. The experimental details are described in the Supporting Information. **Figure S1** presents the ^{1}H NMR spectra ($CDCl_3$-^{d}) of monomer TFMS. The characteristic resonance peaks of vinyl group appeared at 5.46-5.92 and 7.72-7.75 ppm, and all other groups had their corresponding peaks in the ^{1}H NMR spectra, demonstrating that the monomer TFMS was formed. ^{1}H NMR, (400 MHz, δ, $CDCl_3$): 8.17-8.43 (m, 3H of *phenyl*), 7.50-7.53 (q, 1H of -*CH*-), 6.93-7.16 (m, 8H of *phenyl*), 5.44-5.89 (2d, 2H of =CH_2). Mass Spectrometry (MS) (m/z) [M] Calcd for $C_{24}H_{14}O_6F_6$, 512.3; found, 512.3+1.

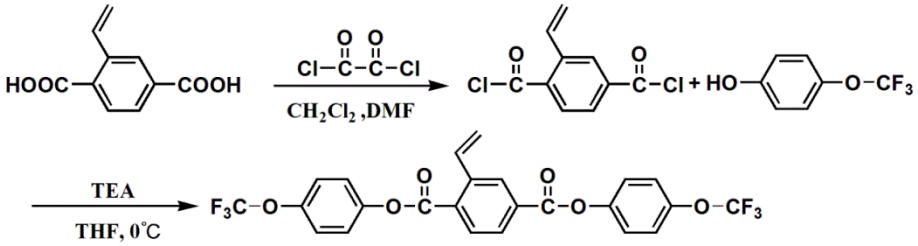

Scheme 1 The synthetic route for the monomer (TFMS)

2.3 Surface functionalization of rGO nanosheets

Fabrication route of core-shell structured rGO@rigid-fluoride-polymer nanosheets is shown in **Scheme 2** and the specific process was as follows: (1) The dried graphene oxide (GO) was thermally exfoliated at 300 °C for 5 min under air and subsequently treated at 800 °C in N_2 for 3 h with a heating rate of 2 ^{o}C/min. The obtained sample was reduced graphene oxide (rGO)[35]. (2) The second step was amino functionalization of rGO. A mass of 0.1 g rGO and 100 ml tetrahydrofuran (THF) were added to a round-bottomed flask and the mixture was sonicated for 30 min. 1.7 g γ-APS was added and the mixture was heated to 80 °C for 24 h under an N_2

atmosphere. The modified rGOs were obtained by centrifugation at 4000 rpm for 5 min, and washed with THF three times and followed by drying under vacuum at 60 °C for 12 h. The amino-functionalized graphene nanosheets (rGO@NH_2) were then formed. (3) The third step was the preparation of graphene anchored by the activation of a RAFT agent (CPDB-NHS) which was synthesized according to the literature [ref]. A mass of 0.1 g of rGO@NH_2 was dispersed in THF and sonicated for 0.5 h, and then the mixture was added dropwise to a THF solution of 0.5 g CPDB-NHS at room temperature while stirring vigorously. After a reaction time of 12 h, the rGO@CPDB was collected by centrifugation and washed with THF three times. Then, the rGO@CPDB was dried at 60°C for 24 h. (4) Finally, the polymer (PTFMS) coated rGO nanosheets via RAFT surface-initiated polymerization from rGO@CPDB were prepared. Two different thicknesses of rGO nanosheets coated by PTFMS were obtained (rGO@PTFMS-1 and rGO@PTFMS-2). The typical procedure was as follows: appropriate quantities of the 0.2g monomers, AIBN, 0.6g rGO@CPDB and refined chlorobenzene were taken in a dry reaction tube containing a magnetic stirring bar. The molar ration of monomer to $N_{monomer} : N_{AIBN} = 20 : 1$, and mass fraction of the monomers was 30%. After three freeze-pump-thaw cycles, the tube was sealed under the vacuum. Polymerization was carried out at 80 °C for 24 h. The sample was purified by centrifugal separation from THF for three times. Finally, the sample was dried under vacuum at 60 °C for 24 h. The prepared sample was denoted as rGO@PTFMS-1. The synthesis of the rGO@PTFMS-2 was similar except for the

$N_{monomer}$:N_{AIBN}=200:1 to obtain a thicker PTFMS shell.

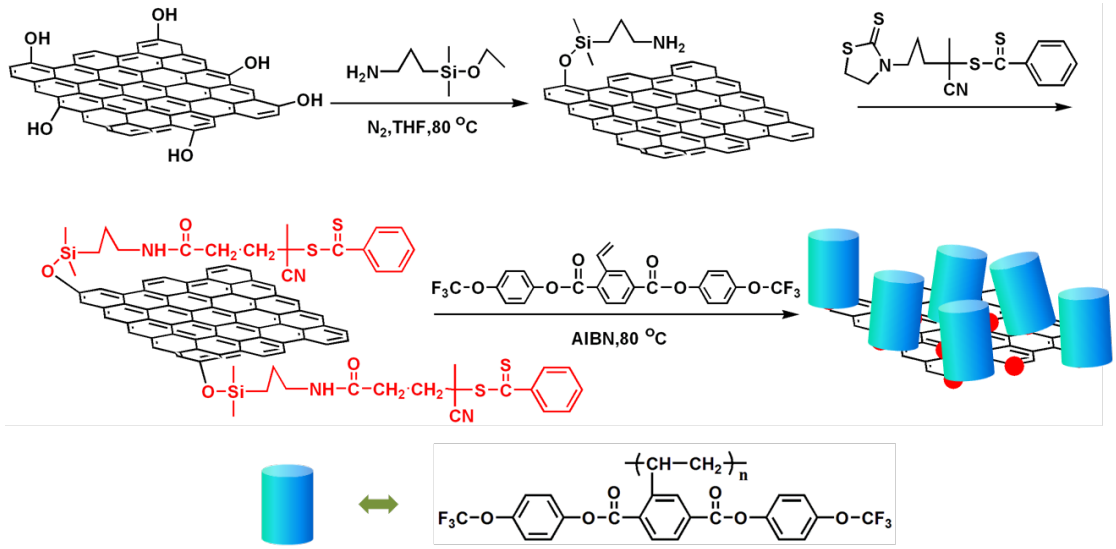

Scheme 2 The fabrication route of the rGO@ rigid-fluoride-polymer

2.4 Cleavage of polymer from functionalization nanosheets

The polymer was cleaved by aminolysis according to the literature [ref]. 30 mg of modified rGO nanosheets, 5 mL THF and 100 μL of HF were added to a centrifuge tube. The mixture was dispersed by sonication for 30 min, and then the mixture was allowed to stir at room temperature for two days. The mixture was filtrated and the solution was evaporated at 60 °C to remove the HF and THF. Finally, the polymer was collected.

2.5 Preparation of rGO@rigid-fluoride-polymer/P(VDF-TrFE-CTFE) nanocomposites films

The typical procedure for the preparation of rGO@rigid-fluoride-polymer/P(VDF-TrFE-CTFE) nanocomposites were carried out as follows: firstly, P(VDF-TrFE-CTFE) was dissolved in a mixed solution DMF/acetone (m/m = 3:7) at room temperature. Secondly, the functional rGO were introduced into the P(VDF-TrFE-CTFE) solution by ball-milling for 24 h. Finally, the uniform suspension was cast onto a clean glass plate to form the nanocomposites films, and then dried under vacuum at 60 °C for 24

h. **Scheme 3** shows the schematic illustration for the formation of the rGO@rigid-fluoride-polymer/P(VDF-TrFE-CTFE) nanocomposites films.

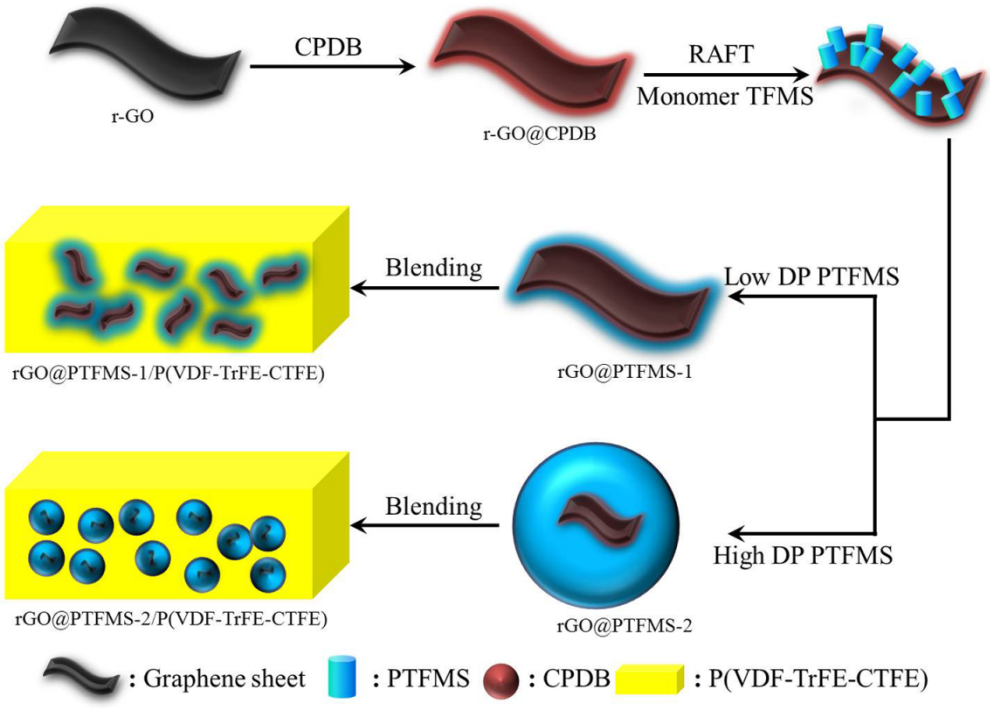

Scheme 3: The fabrication route of rGO@rigid-fluoro-polymer/P(VDF-TrFE-CTFE)

2.6 Characterization

The testing instruments are discussed in the Supporting Information.

3. Results and Discussion

3.1 Synthesis and Characterization of rGO@rigid-fluoride-polymer and nanocomposites

The TFMS monomer was successfully synthesized according to the synthetic route which is illustrated in **Scheme 1**. The ^{1}H NMR spectra (in $CDCl_3$ solvent) of the monomer TFMS, PTFMS and rGO@PTFMS are shown in **Figure 1**. The characteristic resonances of the vinyl group at 5.53 pm and 5.83 pm can be easily seen for the TFMS monomer in **Figure 1**. After polymerization, characteristic resonances

of the vinyl group disappeared completely and the chemical shifts of PTFMS were broadened, which was consistent with the expected polymeric structure. Comparing the characteristic resonances of PTFMS with rGO-PTFMS**,** all characteristic resonances of PTFMS could be found in the ^{1}H NMR graph of rGO@PTFMS, meaning that the rigid-fluoride-polymer PTFMS was coated on the surface of rGO. **Figure 2** presents the FT-IRs of samples and a clear absorption band at 997~1071 cm^{-1} is observed for the rGO@CPDB, originating from thioester bonding. The absorption band at 1645 cm^{-1} and 3000 cm^{-1} were associated with secondary amide bonding and alkyl chain bonding, respectively. These results indicate that the CPDB was successfully introduced onto the surface of the rGO. Compared with pure PTFMS, all absorption bands could be detected in the curve of rGO@PTFMS, implying the rGO nanosheets surfaces were modified by the rigid-fluoride-polymers.

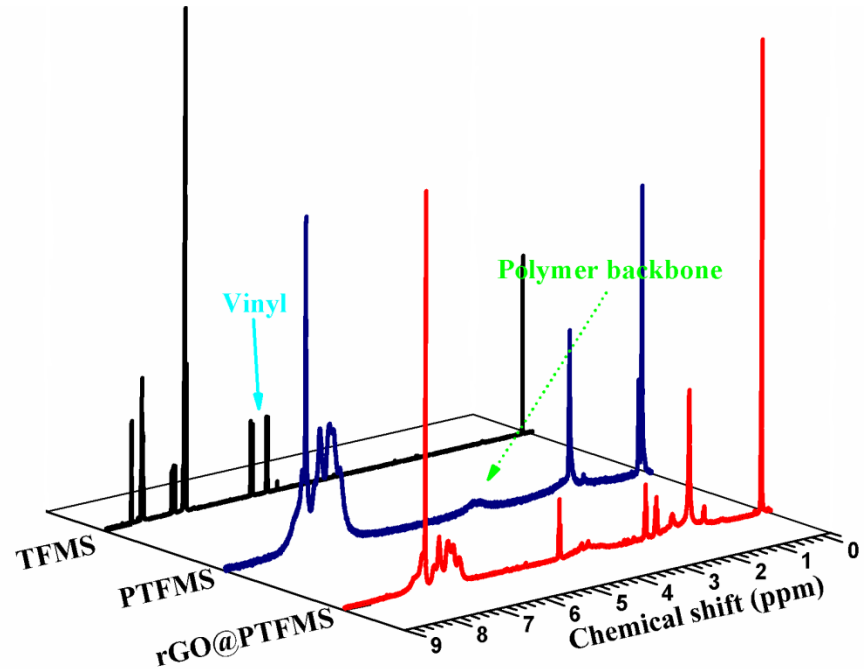

Figure 1. ^{1}H NMR spectra of TFMS monomer, pure polymer PTFMS and rGO@PTFMS in $CDCl_3$

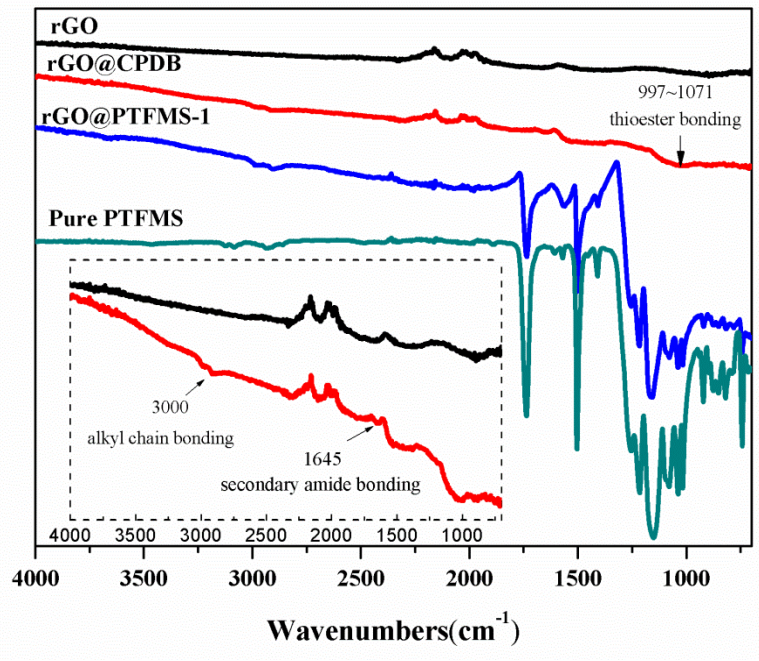

Figure 2. FT-IR spectra of the rGO and its derivatives.

Figure 3 shows the TGA results of the rGO and its derivatives. In this work, two different ratios of rigid-fluoride-monomer were designed to obtain a different shell thickness on the rGO, which were denoted as rGO@PTFMS-1 (thin shell) and rGO@PTFMS-2 (thick shell), respectively. As can be seen in Figure 3, the weight loss of rGO@PTFMS-1 is less than rGO@PTFMS-2, suggesting that the most polymer was grafted onto the rGO surfaces for rGO@PTFMS-2 which has the thickest shell. Based on the TGA results, the weight content of PTFMS in rGO@PTFMS-1 and rGO@PTFMS-2 was calculated using the rGO data as a reference. The results reveal that there was 23 wt % and 59 wt % of PTFMS in rGO@PTFMS-1 and rGO@PTFMS-2, respectively. The results were further confirmed by GPC and AFM. **Table 1** displays the molecular weight and molecular weight distribution of the rigid-fluoride-polymers cleaved from the core-shell structured rGO. The molecular weights of rigid-fluoride-polymers increased from 0.07×10^5 to 1.55×10^5 g/mol for rGO@PTFMS-1 and rGO@PTFMS-2 respectively

and exhibited the same pattern compared to the TGA weight loss, showing the surface-initiated RAFT polymerization is an effective method to control the thickness of polymer shells of rGO. In addition, the liquid crystalline property of cleaved polymers was investigated by POM and 2D WAXD. The results are presented in **Figure 4**. The cleaved polymer from rGO@PTFMS-2 exhibited a strong birefringence phenomenon and a pair of strong diffraction arcs can be seen on the equators at $2\theta=4.98^{o}$ (d-spacing of 1.78 nm) for PTFMS-2 perpendicular to the shear direction. According to the literature [ref] and the experimental results, the polymers PTFMS should form a column nematic phase.

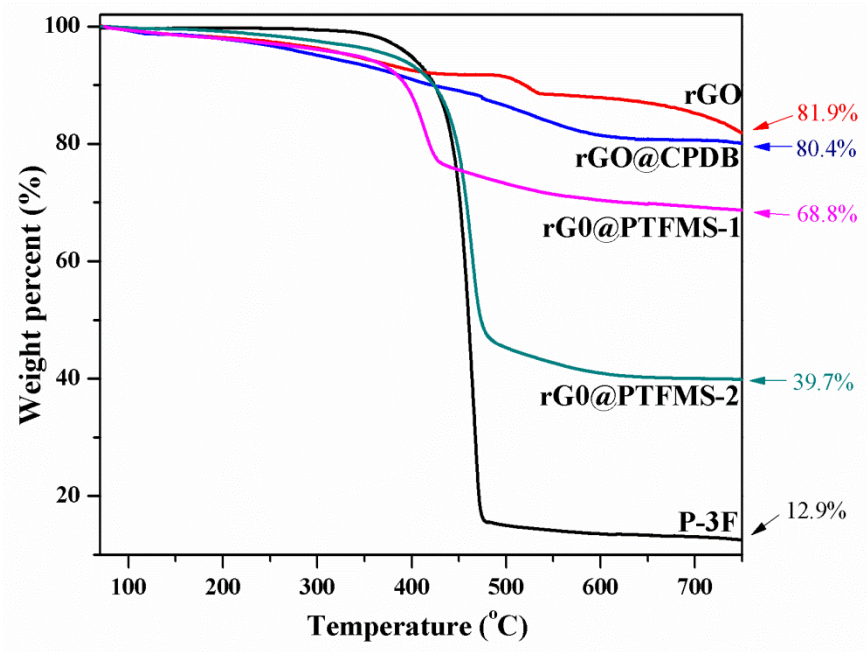

Figure 3. TGA curves of samples in N_2 at a heating rate of 20 ^{o}C min^{-1}

Table 1. Characteristics of the rGO@rigid-fluoride-polymer hybrid nanoparticles

Sample	M_n ($\times 10^{-5}$)	PDI	Calculated thickness	Measure thickness
rGO-PTFMS-1	0.07	1.21	3 nm	2.1 nm
rGO-PTFMS-2	1.75	1.35	71 nm	50 nm

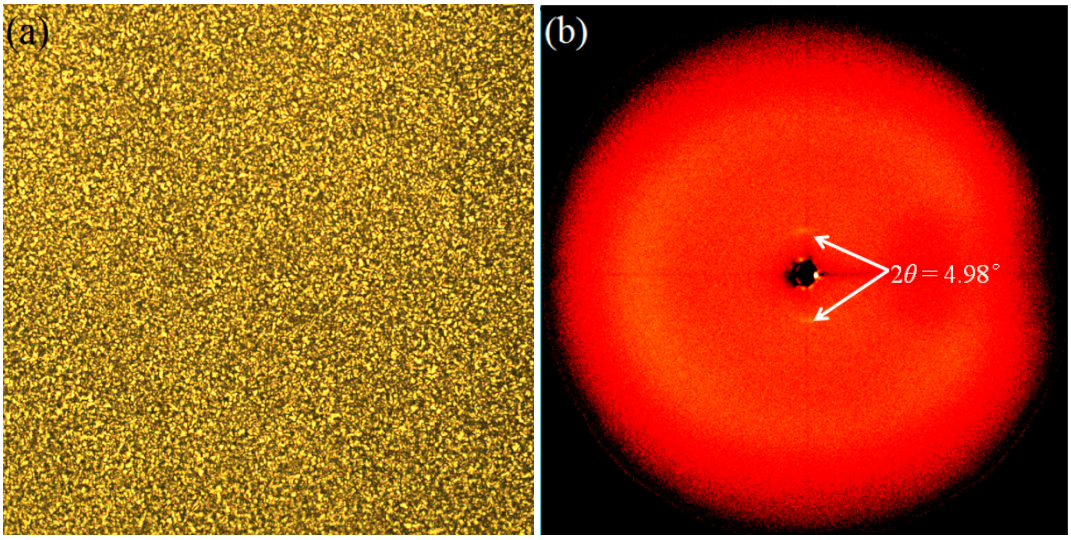

Figure 4. (a) POM image of cleaved polymer PTFMS from rGO@PTFMS-2 at 25 °C, (b) 2D WAXD pattern at room temperature with X-ray beam perpendicular to the direction of the shear. [scale bars?]

AFM was used to directly investigate the morphology and the thickness of the surface functionalized graphene nanofillers. As shown in **Figure 5 (a)**, the individual rGO nanosheet had a thickness of approximately 1.3 nm, which is thicker than that of the ideal graphene[36] due to aggregation of the nanosheets and their poor dispersion in solution. **Figure 5 (b)** shows that rGO@PTFMS-1 exhibits a flat surface profile and the thickness increases to 5.5 nm, indicating that the PTFMS polymer has been uniformly grafted on the surface of rGO. The individual and overall AFM images of rGO@PTFMS-2 are shown in **Figure 5 (c)** and **Figure 5 (d)** respectively. These figures indicate that the thickness sharply increases to 50 nm and a grainy morphology is observed, suggesting that the morphology of the modified rGO changes from nanosheets to nano-granular. TEM can also further observation of the morphologies of rGO derivatives. As shown in the Supporting Information, the surface of the GO sample is relatively smooth. However, the surface of rGO@PTFMS-2 appears to be rough and clearly decorated[37], which is attributed to

the PTFMS coating (see **Figure 5 (e)**). The HR-TEM image of rGO@PTFMS-2 is shown in **Figure 5 (f)** and there are two different textures which represent rGO and PTFMS, confirming the successful preparation of rGO@PTFMS. The thickness of the rigid-fluoro-polymer shells is approximately 2.1 nm for rGO@PTFMS-1 and approximately 50 nm for rGO@PTFMS-2. Compared with the theoretical thickness calculated from equation (1), the actual thickness is in excellent agreement [quote difference %] to the theoretical thickness when the M_n is low, demonstrating the shell thickness can be controlled from the M_n of rigid-polymer. However, there is the slight difference between calculated thickness and measure thickness for rGO@PTFMS-2 when the M_n is high [quote difference %].

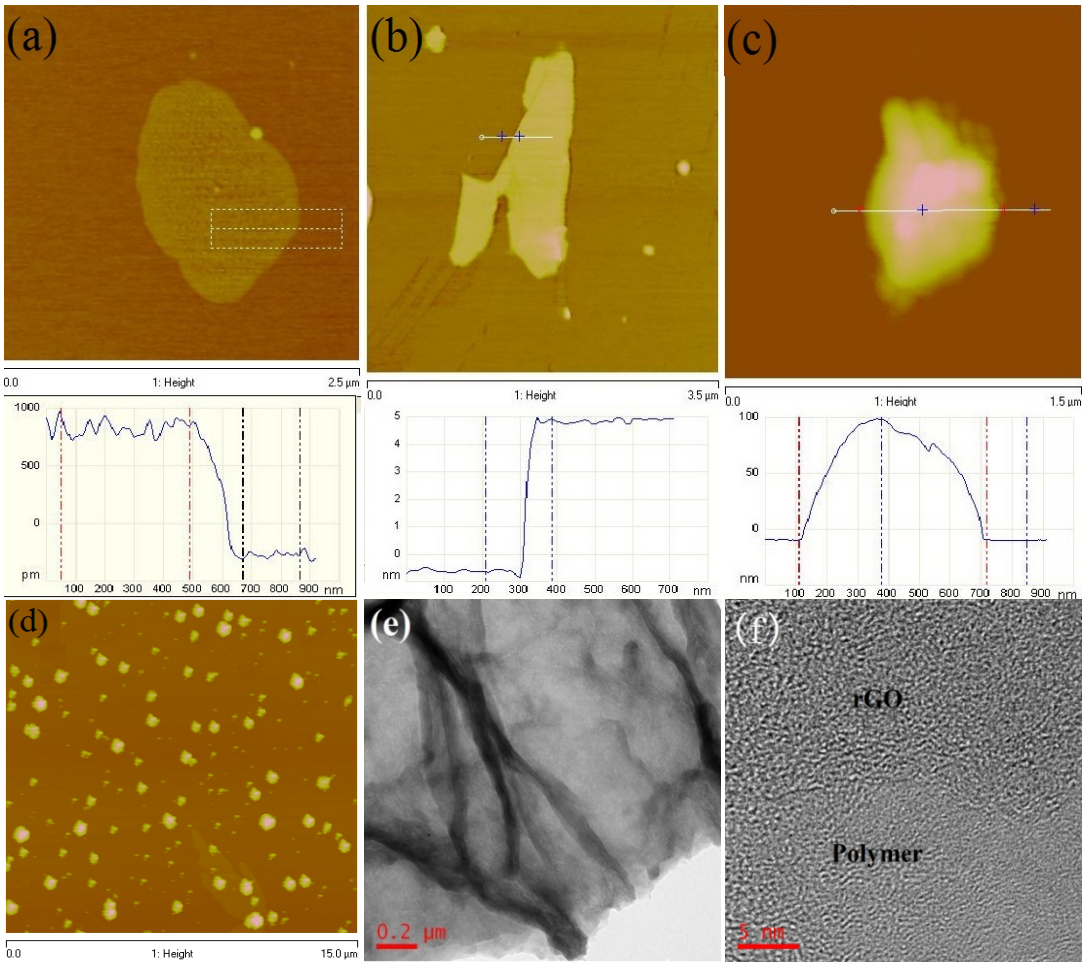

Figure 5. AFM analyses of (a) rGO, (b) rGO@PTFMS-1 and (c), (d) rGO@PTFMS-2. (e) TEM and (f) HR-TEM images of rGO@PTFMS-2.

Freeze-fractured cross-sections of the nanocomposite films were characterized by SEM to investigate the microstructure of the nanocomposites. **Figure 6** shows the SEM images of the fractured surfaces of the pure P(VDF-TrFE-CTFE) and nanocomposite films with different rGO nanofillers. The fracture surface of pure P(VDF-TrFE-CTFE) is rather smooth (**Figure 6 (a)**), while it is rough and ridged for the rGO/P(VDF-TrFE-CTFE) and rGO@PTFMS/P(VDF-TrFE-CTFE) nanocomposite (**Figure 6 (b), (c) and (d)**), resulting from the graphene fillers[38]. It can be seen that the rGO/P(VDF-TrFE-CTFE) nanocomposite films exist a large number of defect and gaps, but the rGO@PTFMS-1/P(VDF-TrFE-CTFE) nanocomposite films have less defects and the rGO@PTFMS-2/P(VDF-TrFE-CTFE) nanocomposite films almost have no defects or gaps. The SEM images of cross-section of rGO@PTFMS-2/P(VDF-TrFE-CTFE) composites films with different rGO@PTFMS-2 loading levels are shown in **Figure 7**. At low filler loadings, it is rather difficult to distinguish the rGO from the polymer matrix, due to its low contrast to the background. As the filler content increases, the rGO become more distinguishable, particularly at a filler content of 1.8 wt %. It can be seen that there are no defect or gaps in the nanocomposites film, and many nanoparticles can be observed, resulting from the rGO@PTFMS-2, which is consistent with the AFM results [link to figure]. These series of images shows the excellent dispersion of rGO-PTFMS and proves the miscibility improvement between the rGO and P(VDF-TrFE-CTFE) matrix via surface functionalization of rGO with PTFMS.

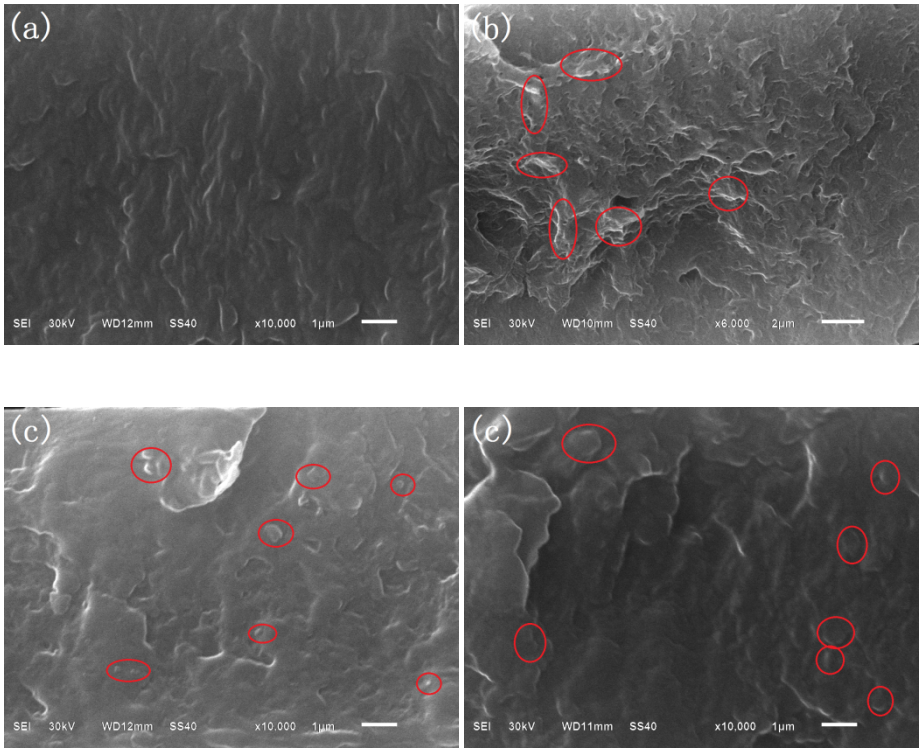

Figure 6. SEM images of cross-section of (a) pure P(VDF-TrFE-CTFE), (b) rGO/P(VDF-TrFE-CTFE) nanocomposite, (c) rGO@PTFMS-1/P(VDF-TrFE-CTFE) nanocomposite, (d) rGO@PTFMS-2/P(VDF-TrFE-CTFE) nanocomposite. Circles indicate.….[loading level?]

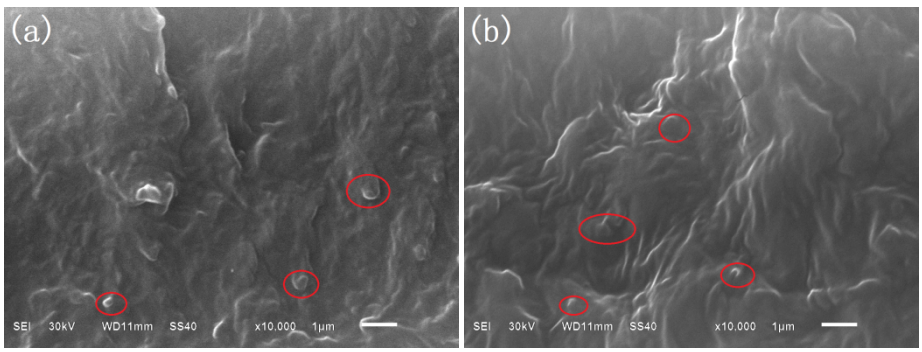

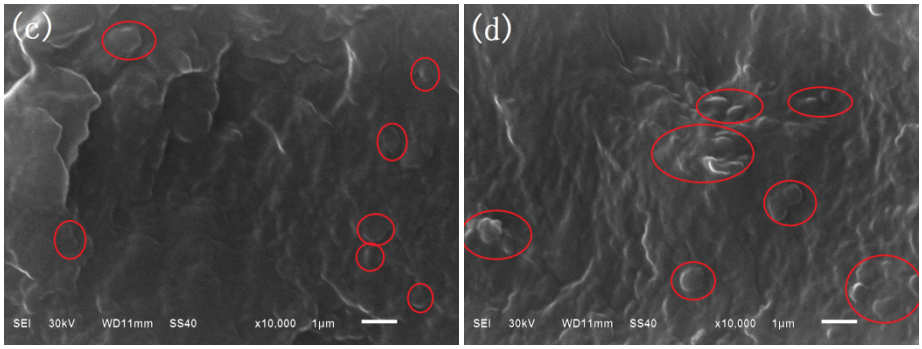

Figure 7. SEM images of cross-section of rGO@PTFMS-2/P(VDF-TrFE-CTFE) composites films with rGO@PTFMS-2 various loading levels: (a) 0.3 wt.%, (b) 0.9wt.%, and (c) 1.5 wt.%, (d) 1.8 wt.%. The scale bar corresponds to 1 μm.

3.2 Dielectric properties of rGO@PTFMS-1/P(VDF-TrFE-CTFE) and rGO@PTFMS-2/ P(VDF-TrFE-CTFE) nanocomposites

The dielectric constant is considered to be a measure of the amount of energy from an external electrical field stored in the material, while the dielectric loss is a measure of the amount of energy dissipated in the dielectric material due to an external electric field. To investigate the dielectric properties of the rGO/P(VDF-TrFE-CTFE) and rGO@PTFMS/ P(VDF-TrFE-CTFE) composites, devices were fabricated with a structure based on gold paste/composites/gold paste and measured with an impedance analyzer. **Figure 8** shows the dielectric constant and dielectric loss of composites at room temperature over a frequency range of 40-10^7 Hz with increasing filler content. As shown in **Figure 8 (a)**, **(c)** and **(e)**, the dielectric constant of each composite decreases with increasing frequency, which can be explained by the polarization relaxation occurring at the inner structure of composites, including interface polarization and dipole orientation polarization. The Maxwell-Wagner effect indicates that the electric charge of a composite will accumulate at the interface because of the different conductivities of each component in an alternating electric field[39-43]. The

dielectric loss of composite measured in the frequency range from 40 to 10^7 Hz at room temperature is shown in **Figure 8 (b)**, **(d)** and **(e)**. The dielectric loss presents two different dielectric behaviors: at low frequency regions the dielectric loss decreases while suddenly increases at high frequency ranges. The low-frequency dielectric response is a typical interface polarization behavior, resulting from heterogeneous interface of the different diphase structures. On the contrary, the high frequency dielectric response is a Debye relaxation behavior derived from the C-F dipole orientation polarization of P(VDF-TrFE-CTFE) matrix[44].

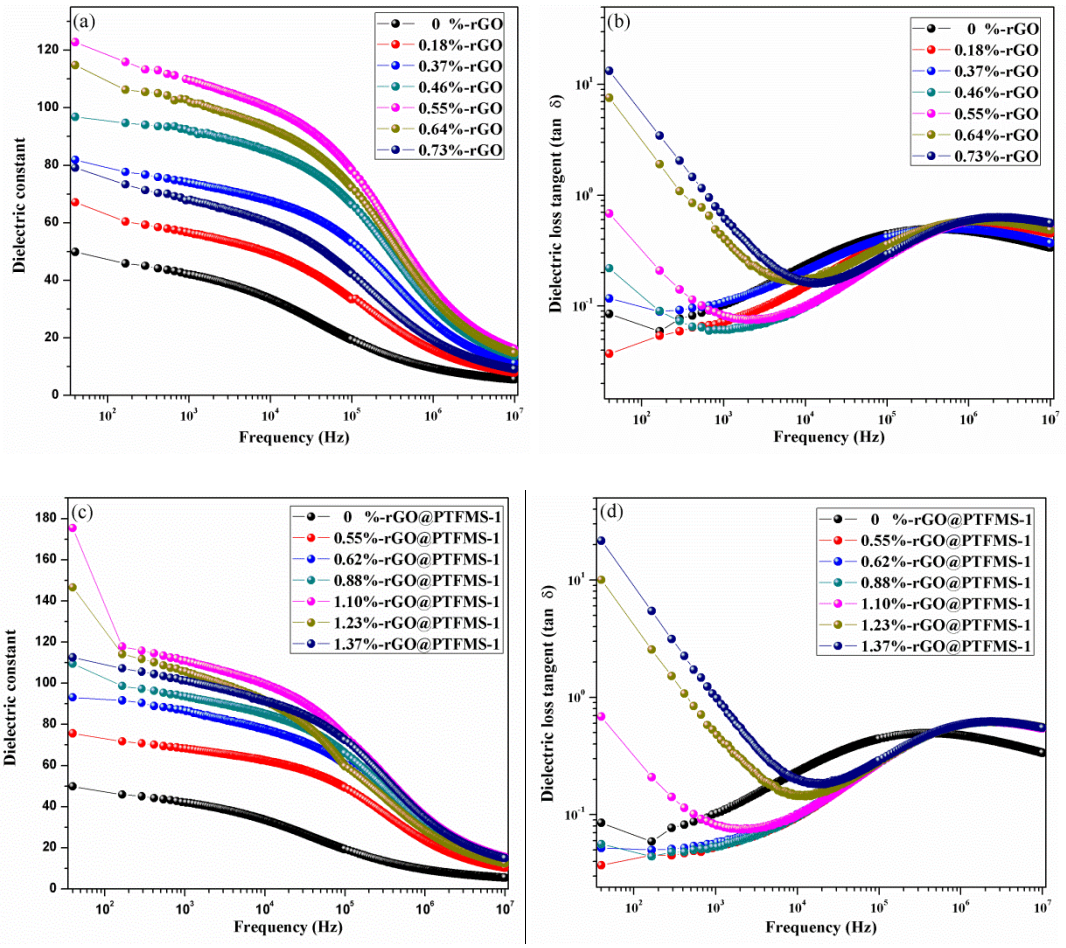

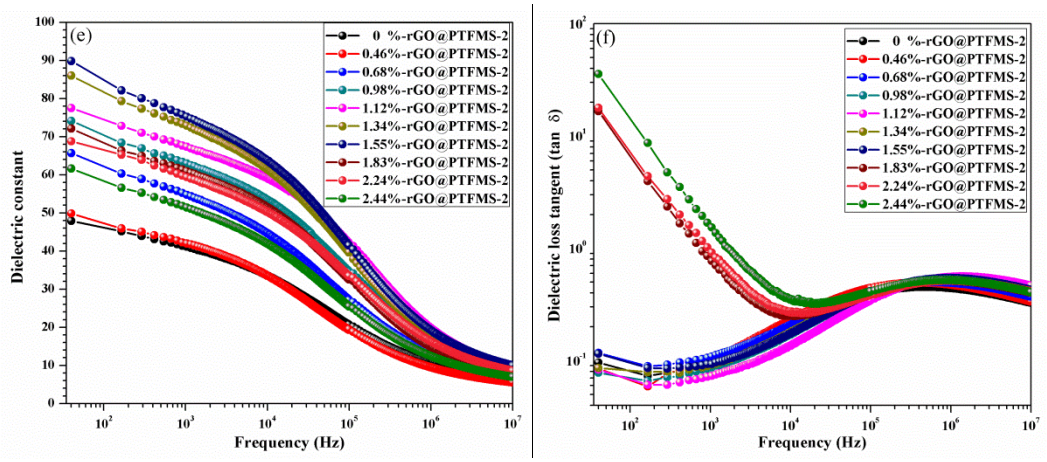

Figure 8. Frequency dependence of the relative permittivity and dielectric loss of the rGO/P(VDF-TrFE-CTFE) and rGO@PTFMS/ P(VDF-TrFE-CTFE) nanocomposites (a) (b) rGO/P(VDF-TrFE-CTFE), (c) (d) rGO@PTFMS-1/ P(VDF-TrFE-CTFE), (e) (f) rGO@PTFMS-2/ P(VDF-TrFE-CTFE).

For an improved understanding, a comparison of the dielectric constant and dielectric loss of rGO/P(VDF-TrFE-CTFE) and rGO@PTFMS/P(VDF-TrFE-CTFE) composites obtained at frequency of 10^3 Hz is shown in **Figure 9**. It can be clearly seen that as the filler contents increases, the dielectric constants of the composite initially increase, then slightly decline. This phenomenon could be understood by the interfacial polarization and percolation theory, where the dielectric properties of the conductive nanofiller/polymer composites depended on the capacitance of the micro-capacitors formed by conductive rGO nanosheets as plates in the P(VDF-TrFE-CTFE)as matrix[45-47]. Schematics of the microstructures of the rGO@PTFMS/P(VDF-TrFE-CTFE) composites with thin and thick shells with an increase of rGO@PTFMS mass fractions are shown in **Figure 9**. **Secondly**, the dielectric constant of rGO@PTFMS-2/P(VDF-TrFE-CTFE) composite is lower than that of rGO/P(VDF-TrFE-CTFE) and rGO@PTFMS-1/P(VDF-TrFE-CTFE) composites since the rGO@PTFMS-2 has the thickest shell of functional polymers

(PTFMS). This result can be understood by the following explanation: the traditional two-dimensional planar structure of rGO changes to nanoparticle structure, which is shown in **Scheme 3**. The formation of micro-capacitors is weakened and the numbers of micro-capacitor decrease, thus resulting in the decreasing of the dielectric constant. **Thirdly,** owning to high surface energy feature of graphene sheets, the adjoining graphene sheets tend to agglomerate together rather than disperse in the P(VDF-TrFE-CTFE) matrix uniformly, thus the average thickness of PVDF matrix between two micro-capacitor plates is large and the capacitance is therefore smaller [48]. As shown above, the surface functional PTFMS can dramatically improve the interfacial bonding between the graphene nanosheets and polymer matrix, resulting in a decrease in nanofiller aggregation. The microstructure of rGO@PTFMS-1/P(VDF-TrFE-CTFE) composites with a low rGO@PTFMS-1 content is illustrated in **Figure 10 (a)**, where the micro-capacitors are separated from each other. With the increase of the content of fillers, new micro-capacitor formed as a result of the addition of rGO@PTFMS. When the contents of fillers is close to the critical (percolation) value, the distance between the graphene sheets decrease and the number of micro-structure rises, which will leads to an enhanced dielectric constant. However, as the fraction of filler exceeds the critical value, due to the Van der Waals forces and π-π interaction among the fillers, the surface functional fillers in P(VDF-TrFE-CTFE) will aggregate and contact each other to form conductive paths[49, 50], as in **Figure 10 (c)**. According to the micro-capacitor model, the expected number of capacitors in the composites will be reduced because of the aggregation of fillers, leading to a lower dielectric constants. Finally, as the percolation threshold of nanocomposites increased from 0.55 vol % to 1.55 vol % with the increment of shell thickness. In the rGO/P(VDF-TrFE-CTFE) nanocomposites film, the agglomeration, pores and defects caused by the

rGOs can sharply increase the local electric field, resulting in the increasing of interfacial polarization and lower the percolation threshold. The rGO@PTFMS-2/P(VDF-TrFE-CTFE) composite exhibited the highest percolation threshold due to the insulating polymer PTFMS and the decreasing number of micro-capacitors. The same percolation threshold is observed in the dielectric loss curves, Figure 9b?. On reaching to the percolation threshold, the dielectric loss of nanocomposites sharply increase due to increase of conduction loss (see Supporting Information).

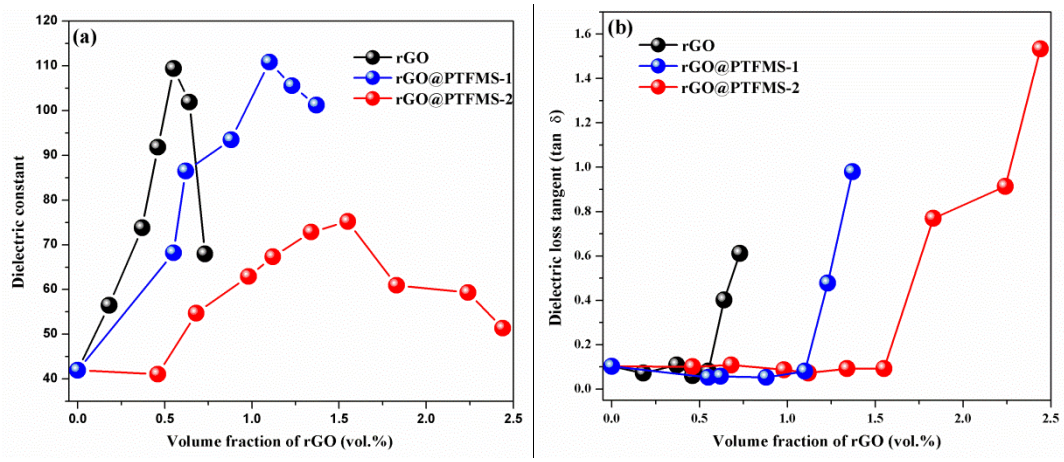

Figure 9. The dependence of the (a) dielectric constant and (b) dielectric loss of the composites on the filler volume fraction, measured at room temperature and 1 kHz.

For the composites filled with conductive graphene nanosheets, the dielectric permittivity of the composite can be predicted by the following percolation theory power law[51], where ε is the dielectric constant of the composite, ε_m is the dielectric permittivity of the P(VDF-TrFE-CTFE) matrix (in this work ε_m = 41.9 at 1 kHz), f_{rGO} is the volume fraction of rGO in the composite, f_c is the critical volume fraction of the rGO at the percolation threshold, S is the critical exponent related to the material properties.

$$\varepsilon = \varepsilon_m (f_c - f_{rGO})^{-S}, \text{ for } f_{rGO} < f_c \qquad (2)$$

According to the formula (2), the best fit curve for the experimental dielectric constants of the composites was carried out and the results are shown in **Figure 11**. Fitting leads to f_c values for the rGO/P(VDF-TrFE-CTFE) , rGO@PTFMS-1/P(VDF-TrFE-CTFE) and rGO@PTFMS-2/P(VDF-TrFE-CTFE) composites to be 0.61 vol.%, 1.21 vol.% and 1.69vol.%, respectively, which is in good agreement with the experiment value. [I guess it would fit as you use the experimental data to fit?, 11bc not so good? Interesting the cruve changes sign experimentally?]

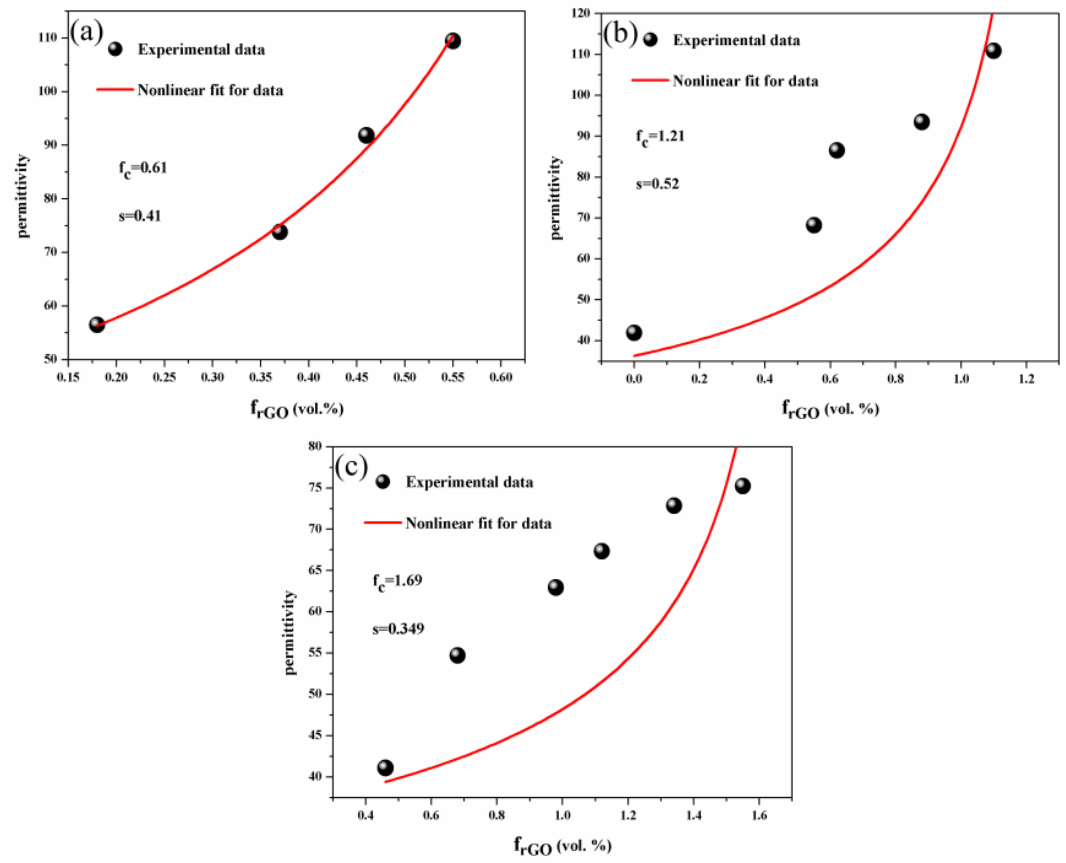

Figure 11: The determination of percolation threshold of composites with different volume fraction of (a) rGO, (b) rGO@PTFMS-1 and (c) rGO@PTFMS-2 in P(VDF-TrFE-CTFE) matrix The results were calculated based on the best linear fit for experimental dielectric constant data acquired at 1kHz.

4. Conclusion

In this work, a rigid-fluoride-polymer functionalized reduced graphene oxide (rGO) was successfully prepared by RAFT in situ polymerization. The P(VDF-TrFE-CTFE) matrix nanocomposites filled with rGO, can core-shell strucutures of rGO@PTFMS-1 (thin shell) and rGO@PTFMS-2 (thick shell) were fabricated and their dielectric properties were investigated. Our results demonstrated that the grafting of rGO@PTFMS can effectively enhanced the dispersion and compatibility of the rGO nanofillers in the P(VDF-TrFE-CTFE) matrix. Additionally, the surface-grafted PTFMS polymer can be entangled with the polymer chains of the matrix, which can further influence the interfacial adhesion between rGO and the polymer matrix. Dielectric measurements revealed that the percolation threshold of rGO@PTFMS-1/P(VDF-TrFE-CTFE) is 1.21vol.%, which was lower than that of rGO@PTFMS-2/P(VDF-TrFE-CTFE) and higher than that of rGO/P(VDF-TrFE-CTFE). When the rGO or modified rGO volume fraction is near the percolation threshold, the nanocomposites produce the highest dielectric constant. More importantly, the 2-D morphology of graphene nanofiller was changed to a granular structure through surface decoration of liquid-crystalline polymer with crowded, rigid, and bulky side groups (PTFMS), leading to the highest percolation threshold. These results suggest that the fluoride-liquid-crystalline polymer functionalized rGO is a promising candidate for tailoring the dielectric properties of the polymer nanocomposites.

Acknowledgements

This research was financially supported by the National Nature Science Foundation of China (21504075) and Nature Science Foundation of Hunan Provinces (2017JJ3294).

References

[1] B. Chu, X. Zhou, K. Ren, B. Neese, M. Lin, Q. Wang, et al. A dielectric polymer with high electric energy density and fast discharge speed. Science. 2006;313(5785):334-336.

[2] M.N. Nadagouda, R.S. Varma. Green approach to bulk and template-free synthesis of thermally stable reduced polyaniline nanofibers for capacitor applications. Green Chemistry. 2007;9(6):632-637.

[3] D. Wang, T. Zhou, J.W. Zha, J. Zhao, C.J. Shi, Z.M. Dang. Functionalized graphene–$BaTiO_3$/ferroelectric polymer nanodielectric composites with high permittivity, low dielectric loss, and low percolation threshold. Journal of materials Chemistry A. 2013;1(20):6162-6168.

[4] Q. Li, K. Han, M.R. Gadinski, G. Zhang, Q. Wang. High Energy and Power Density Capacitors from Solution□Processed Ternary Ferroelectric Polymer Nanocomposites. Advanced Materials. 2014;26(36):6244-6249.

[5] P. Hu, Y. Song, H. Liu, Y. Shen, Y. Lin, C.W. Nan. Largely enhanced energy density in flexible P (VDF-TrFE) nanocomposites by surface-modified electrospun $BaSrTiO_3$ fibers. Journal of Materials Chemistry A. 2013;1(5):1688-1693.

[6] H. Luo, D. Zhang, C. Jiang, X. Yuan, C. Chen and K. C. Zhou. Improved dielectric properties and energy storage density of poly(vinylidene fluoride-co-hexafluoropropylene) nanocomposite with hydantoin epoxy resin coated $BaTiO_3$, ACS Applied Materials & Interfaces, 2015; 7(15): 8061-8069.

[7] Q. Li, F. Liu, T. Yang, M.R. Gadinski, G. Zhang, L.Q. Chen, et al. Sandwich-structured polymer nanocomposites with high energy density and great charge–discharge efficiency at elevated temperatures. Proceedings of the National Academy of Sciences. 2016;113(36):9995-10000.

[8] H. Tang, Z. Zhou, C.C. Bowland, H.A. Sodano. Synthesis of calcium copper titanate ($CaCu_3Ti_4O_{12}$) nanowires with insulating SiO_2 barrier for low loss high dielectric constant nanocomposites. Nano Energy. 2015;17:302-307.

[9] H. Tang, Y. Lin, H.A. Sodano. Enhanced energy storage in nanocomposite capacitors through aligned PZT nanowires by uniaxial strain assembly. Advanced Energy Materials. 2012;2(4):469-476.

[10] L. Liu, Y. Zhang, F. Lv, W. Tong, L. Ding, P.K. Chu, et al. Polyimide composites composed of covalently bonded $BaTiO_3$@GO hybrids with high dielectric constant and low dielectric loss. RSC Advances. 2016;6(90):86817-86823.

[11] S. Liu, J. Zhai. Improving the dielectric constant and energy density of poly (vinylidene fluoride) composites induced by surface-modified $SrTiO_3$ nanofibers by polyvinylpyrrolidone. Journal of Materials Chemistry A. 2015;3(4):1511-1517.

[12] Q.G. Chi, J.F. Dong, C.H. Zhang, C.P. Wong, X. Wang, Q.Q. Lei. Nano iron oxide-deposited calcium copper titanate/polyimide hybrid films induced by an external magnetic field: toward a high dielectric constant and suppressed loss. Journal of Materials Chemistry C. 2016;4(35):8179-8188.

[13] Z.M. Dang, M.S. Zheng, J.W. Zha. 1D/2D Carbon Nanomaterial□Polymer Dielectric Composites with High Permittivity for Power Energy Storage Applications. Small. 2016;12(13):1688-1701.

[14] Q. Zhuang, X. Mao, Z. Xie, X. Liu, Q. Wang, Y. Chen, et al. Synthesis of multiwalled carbon nanotube/fluorine□containing poly (p□phenylene benzoxazole) composites exhibiting greatly enhanced dielectric constants. Journal of Polymer Science Part A: Polymer Chemistry. 2012;50(22):4732-4739.

[15] H. Luo, K. C. Zhou, C. R. Bowen, F. Q. Zhang, A. Q. Wei, Z. Wu, et al. Building hierarchical interfaces using $BaSrTiO_3$ nanocuboid dotted graphene sheets in

an optimized percolative nanocomposite with outstanding dielectric properties. Advanced Materials Interfaces, 2016; 1600157.

[16] X. Peng, W. Xu, L. Chen, Y. Ding, S. Chen, X. Wang, et al. Polyimide complexes with high dielectric performance: toward polymer film capacitor applications. Journal of Materials Chemistry C. 2016;4(27):6452-6456.

[17] F. Bonaccorso, L. Colombo, G. Yu, M. Stoller, V. Tozzini, A.C. Ferrari, et al. Graphene, related two-dimensional crystals, and hybrid systems for energy conversion and storage. Science. 2015;347(6217):1246501.

[18] L. Zhang, K. Zhao, W. Xu, Y. Dong, R. Xia, F. Liu, et al. Integrated SnO_2 nanorod array with polypyrrole coverage for high-rate and long-life lithium batteries. Physical Chemistry Chemical Physics. 2015;17(12):7619-7623.

[19] B. Luo, L. Zhi. Design and construction of three dimensional graphene-based composites for lithium ion battery applications. Energy & Environmental Science. 2015;8(2):456-477.

[20] D.H. Lan, L. Chen, C.T. Au, S.F. Yin. One-pot synthesized multi-functional graphene oxide as a water-tolerant and efficient metal-free heterogeneous catalyst for cycloaddition reaction. Carbon. 2015;93:22-31.

[21] R.K. Layek, A.K. Das, M.J. Park, N.H. Kim, J.H. Lee. Enhancement of physical, mechanical, and gas barrier properties in noncovalently functionalized graphene oxide/poly (vinylidene fluoride) composites. Carbon. 2015;81:329-338.

[22] F. Caruso. Nanoengineering of particle surfaces. Advanced materials. 2001;13(1):11-22.

[23] H. Li, Z. Chen, L. Liu, J. Chen, M. Jiang, C. Xiong. Poly (vinyl pyrrolidone)-coated graphene/poly (vinylidene fluoride) composite films with high dielectric permittivity and low loss. Composites Science and Technology. 2015;121:49-55.

[24] Y.J. Wan, W.H. Yang, S.H. Yu, R. Sun, C.P. Wong, W.H. Liao. Covalent polymer functionalization of graphene for improved dielectric properties and thermal stability of epoxy composites. Composites Science and Technology. 2016;122:27-35.

[25] J.Y. Wang, S.Y. Yang, Y.L. Huang, H.W. Tien, W.K. Chin, C.C.M. Ma. Preparation and properties of graphene oxide/polyimide composite films with low dielectric constant and ultrahigh strength via in situ polymerization. Journal of Materials Chemistry. 2011;21(35):13569-13575.

[26] J. Tong, H.X. Huang, M. Wu. Facile green fabrication of well dispersed poly (vinylidene fluoride)/graphene oxide nanocomposites with improved properties. Composites Science and Technology. 2016;129:183-190.

[27] Y. Chen, S. Zhang, X. Liu, Q. Pei, J. Qian, Q. Zhuang, et al. Preparation of solution-processable reduced graphene oxide/polybenzoxazole nanocomposites with improved dielectric properties. Macromolecules. 2015;48(2):365-372.

[28] K. Yang, X. Huang, L. Fang, J. He, P. Jiang. Fluoro-polymer functionalized graphene for flexible ferroelectric polymer-based high-k nanocomposites with suppressed dielectric loss and low percolation threshold. Nanoscale. 2014;6(24):14740-14753.

[29] C. Wu, X. Huang, G. Wang, X. Wu, K. Yang, S. Li, et al. Hyperbranched-polymer functionalization of graphene sheets for enhanced mechanical and dielectric properties of polyurethane composites. Journal of Materials Chemistry. 2012;22(14):7010-7019.

[30] R.K. Layek, S. Samanta, D.P. Chatterjee, A.K. Nandi. Physical and mechanical properties of poly (methyl methacrylate)-functionalized graphene/poly (vinylidine fluoride) nanocomposites: Piezoelectric β polymorph formation. Polymer. 2010;51(24):5846-5856.

[31] C. Yang, S.J. Hao, S.L. Dai, X.Y. Zhang. Nanocomposites of poly (vinylidene fluoride)-Controllable hydroxylated/carboxylated graphene with enhanced dielectric performance for large energy density capacitor. Carbon. 2017;117:301-312.

[32] Q.F. Zhou, H.M. Li, X.D. Feng. Synthesis of liquid-crystalline polyacrylates with laterally substituted mesogens. Macromolecules. 1987;20(1):233-234.

[33] H. Luo, C. Ma, X.F. Zhou, S. Chen, D. Zhang Interfacial Design in Dielectric Nanocomposite Using Liquid-Crystalline Polymers Macromolecules 2017,50: 5132-5137

[34] C. Li, J. Han, C.Y. Ryu, B.C. Benicewicz. A versatile method to prepare RAFT agent anchored substrates and the preparation of PMMA grafted nanoparticles. Macromolecules. 2006;39(9):3175-3183.

[35] Q. Du, M. Zheng, L. Zhang, Y. Wang,J. Chen, L. Xue, et al. Preparation of functionalized graphene sheets by a low-temperature thermal exfoliation approach and their electrochemical supercapacitive behaviors. Electrochimica Acta. 2010;55(12):3897-3903.

[36] D.R. Dreyer, S. Park, C.W. Bielawski, R.S. Ruoff. The chemistry of graphene oxide. Chemical Society Reviews. 2010;39(1):228-240.

[37] K. Yang, X. Huang, L. Fang, J. He, P. Jiang. Fluoro-polymer functionalized graphene for flexible ferroelectric polymer-based high-k nanocomposites with suppressed dielectric loss and low percolation threshold. Nanoscale. 2014;6(24):14740-14753.

[38] L.B. Zhang, J.Q. Wang, H.G. Wang, Y. Xu, Z.F. Wang, Z.P. Li, et al. Preparation, mechanical and thermal properties of functionalized graphene/polyimide nanocomposites. Composites Part A: Applied Science and Manufacturing. 2012;43(9):1537-1545.

[39] H. Luo, Z. Wu, C. Chen, K. C. Zhou, and D. Zhang. Methoxypolyethylene glycol functionalized carbon nanotube composites with high permittivity and low dielectric loss. Composites Part A, 2016; 86: 57-65.

[40] T. Zhou, J.W. Zha, R.Y. Cui, B.H. Fan, J.K. Yuan, Dang Z-M. Improving dielectric properties of $BaTiO_3$/ferroelectric polymer composites by employing surface hydroxylated $BaTiO_3$ nanoparticles. ACS applied materials & interfaces. 2011;3(7):2184-2188.

[41] S.h. Liu, J.W. Zhai, J.W. Wang, S.X. Xue, W.Q. Zhang. Enhanced energy storage density in poly (vinylidene fluoride) nanocomposites by a small loading of suface-hydroxylated $Ba_{0.6}Sr_{0.4}TiO_3$ nanofibers. ACS applied materials & interfaces. 2014;6(3):1533-1540.

[42] X. Li, Y.F. Lim, K. Yao, F.E.H. Tay, K.H. Seah. Ferroelectric poly (vinylidene fluoride) homopolymer nanotubes derived from solution in anodic alumina membrane template. Chemistry of Materials. 2013;25(4):524-529.

[43] G. Hu, F. Gao, J. Kong, S. Yang, Q. Zhang, Z. Liu, et al. Preparation and dielectric properties of poly (vinylidene fluoride)/$Ba_{0.6}Sr_{0.4}TiO_3$ composites. Journal of Alloys and Compounds. 2015;619:686-692.

[44] C. Chanmal, J. Jog. Dielectric relaxations in PVDF/$BaTiO_3$ nanocomposites. Express Polymer Letters. 2008;2(4):294-301.

[45] M. Li, X. Huang, C. Wu, H. Xu, P. Jiang, T. Tanaka. Fabrication of two-dimensional hybrid sheets by decorating insulating PANI on reduced graphene oxide for polymer nanocomposites with low dielectric loss and high dielectric constant. Journal of Materials Chemistry. 2012;22(44):23477-23484.

[46] Z.M. Dang, L. Wang, Y. Yin, Q. Zhang, Q.Q. Lei. Giant dielectric permittivities in functionalized carbon□nanotube/electroactive□polymer nanocomposites. Advanced Materials. 2007;19(6):852-857.

[47] X. Huang, P. Jiang, L. Xie. Ferroelectric polymer/silver nanocomposites with high dielectric constant and high thermal conductivity. Applied Physics Letters. 2009;95(24):242901.

[48] L. Chu, Q. Xue, J. Sun, F. Xia, W. Xing, D. Xia, et al. Porous graphene sandwich/poly (vinylidene fluoride) composites with high dielectric properties. Composites Science and Technology. 2013;86:70-75.

[49] Y. Bai, Z.Y. Cheng, V. Bharti, H. Xu, Q. Zhang. High-dielectric-constant ceramic-powder polymer composites. Applied Physics Letters. 2000;76(25):3804-3806.

[50] X.L. Xu, C.J. Yang, J.H. Yang, T. Huang, N. Zhang, Y. Wang, et al. Excellent dielectric properties of poly (vinylidene fluoride) composites based on partially reduced graphene oxide. Composites Part B: Engineering. 2017;109:91-100.

[51] D. Wang, Y. Bao, J.W. Zha, J. Zhao, Z.M. Dang, G.H. Hu. Improved dielectric properties of nanocomposites based on poly (vinylidene fluoride) and poly (vinyl alcohol)-functionalized graphene. ACS applied materials & interfaces. 2012;4(11):6273-6279.